A Method for Deriving Tone Noise Information from CFD Calculations on the Aeroengine Fan Stage

A.G. Wilson
Rolls-Royce plc
ML 81
P.O. Box 31, Moor Lane
Derby, DE24 8BJ
United Kingdom

Abstract

A wavesplitting procedure is proposed by which noise information can be derived from CFD calculations on the aeroengine fan stage. Noise propagation in the ducted regions is compared with well-understood linear behaviour in parallel wall ducts. Deviations from this behaviour are used to highlight important features of the flow solution. These include genuine flow features such as non-linear acoustic interaction as well as dissipation and boundary condition errors deriving from the numerical solution of the equations. Properly applied, the method provides quantitative noise source amplitudes, accounting for (modest) reflections from the boundaries of the CFD domain. At the same time confidence can be gained that the CFD results are accurate for the wavelengths and frequencies being analysed, and that the CFD domain sufficiently covers the region of interest.
Examples are given of how the method can be applied to steady and unsteady CFD calculations. Limitations of the method are also discussed.

Introduction

Wavesplitting (decomposition of a flow field into upstream and downstream travelling eigenmodes) is widely used in CFD boundary conditions to determine the direction in which information is travelling, and hence to prevent spurious reflections at the boundaries of the domain. Tyler and Sofrin (1961) first derived the acoustic modes for uniform axial flow in cylindrical and annular ducts. This formulation has been widely and successfully applied to boundary conditions: Giles, for example, used the modes with varying levels of approximation to produce 1D and 2D non-reflecting conditions (Giles 1990, Saxer and Giles 1993). Other authors have proposed a complete 3D formulation. The method has, however, clear limitations. Ducts are not in general parallel annulus. Flow is generally non-uniform radially. Amplitudes (particularly with regard to rotor alone tones) are so high that the acoustic perturbations behave non-linearly (Morfey and Fisher 1970). Moreover, in addition to these physical features, CFD solutions have their own characteristics: smoothing, grid and boundary conditions all affect the noise prediction process. Rowley and Colonius (1998) developed numerically non-reflecting boundary conditions by calculating linear modes using the true mean flow profile and included in their analysis the discretisation of the particular CFD code being used.
In this paper a wavesplitting method is developed for use *inside* the computational domain, as an aid to deriving tone noise information from the CFD solution. As with the boundary conditions, a decision has to be made as to the complexity required. 1D and 2D analyses are insufficient for the general case. Instead a 3D uniform axial flow method based on Tyler and Sofrin modes is adopted. This has many advantages over more complex methods:

- The modes can be calculated quickly using standard Bessel functions.
- The modes are orthogonal, making decomposition easier and faster.
- The behaviour of the Tyler and Sofrin modes is well understood.
- The resulting wavesplitting routines are general across all CFD codes.

Paper presented at the RTO AVT Symposium on "Ageing Mechanisms and Control: Part A – Developments in Computational Aero- and Hydro-Acoustics", held in Manchester, UK, 8-11 October 2001, and published in RTO-MP-079(I).

Two methods are given for splitting the flow field at a given axial plane into Tyler and Sofrin modes, depending on whether or not vortical as well as acoustic waves are present in the flow. The output of each method is a number representing amplitude and phase for the upstream and downstream travelling acoustic waves at each circumferential and radial harmonic.

Tyler and Sofrin modes propagate either at constant amplitude (cut-on waves) or with log amplitude varying linearly with axial distance (cut-off waves). In both cases the phase varies linearly with distance. The axial wavenumber, representing the rate of change of amplitude and phase, can be calculated analytically from the circumferential wavenumber, the wave frequency and the (axial) Mach number of the mean flow (appendix 1). Because the Tyler and Sofrin modes do not agree exactly with either the physical or the CFD calculated modes (for the reasons outlined above), the behaviour of the calculated wave amplitude varies from this 'ideal'. By plotting log amplitude and phase against axial distance it is possible to isolate these regions, and hence to direct further work at establishing whether the cause of the discrepancy is physical (eg non-linearity, hade angle, non-uniform mean flow) or numerical (eg dissipation error, reflections from the boundaries). This has proved an essential step in obtaining reliable noise information, and the examples below show how the analysis might proceed from the basic method to derive quantitative estimates of source noise.

Example 1: Steady CFD, Boundary Conditions, Non-linear effects

Before describing the mechanics of the method it is useful to consider an example to illustrate the progression of thought. Fig 1 shows the result of a steady CFD calculation of a research fan blade at rig scale, aimed at predicting fan-forward rotor alone noise. The pressure has been Fourier transformed circumferentially to decompose it into the harmonics of blade passing frequency that would be detected by a stationary microphone at the outer wall. The signal amplitude at the first blade passing harmonic is plotted on a log scale (in fact, as Sound Pressure Level, SPL[1]) against distance upstream of the fan tip leading edge. The large oscillations in amplitude are known from measurements to be false.

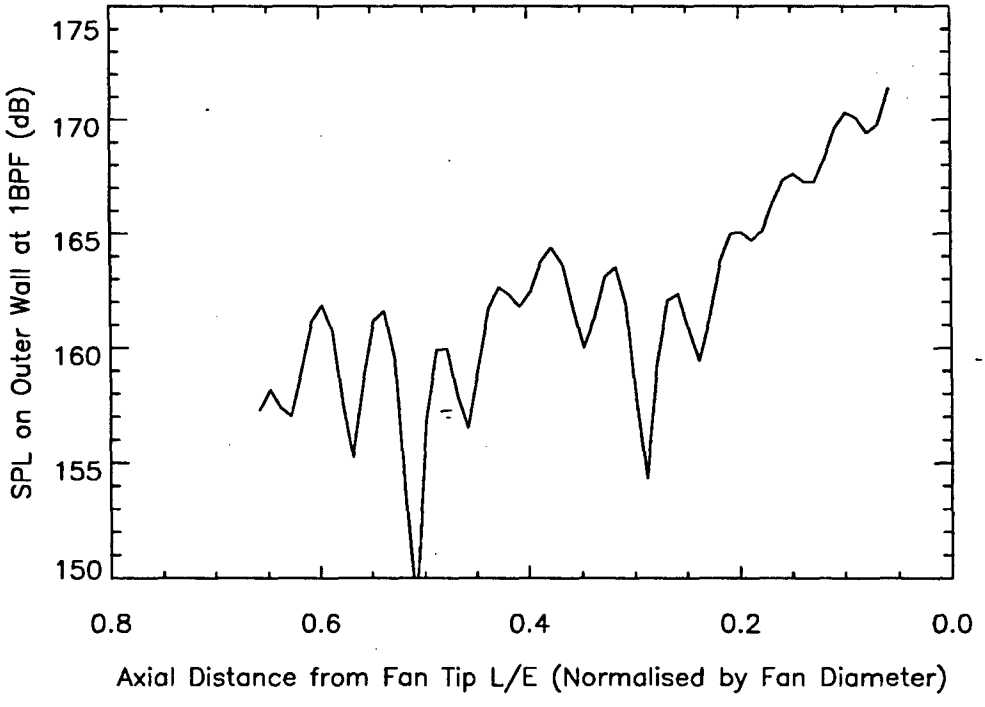

Figure 1. Steady CFD Solution for Fan Rotor Alone Noise; SPL on Outer Wall

[1] Sound Pressure Level (SPL) is defined in the usual way as $20\log_{10}(\text{Prms}/\ 2.10^{-5}\text{Pa})$

The starting strength close to the fan is known to be roughly correct, but the signal (if genuine) is contaminated by oscillations in the solution, making it hard to quantify the noise produced. Two lengthscales can be distinguished; a short wavelength oscillation with about eleven peaks over the axial domain, and a longer wavelength oscillation with troughs at x=0.5 and x=0.3.

The first step in the analysis procedure is to split the pressure signal into Bessel-Fourier harmonics. It will be seen later that over the majority of the domain the first radial harmonic dominates the signal at the outer wall. This harmonic is shown as the long dashes in fig 2, compared to the outer wall values from fig 1. The longer lengthscale oscillation has disappeared, leaving a smoothly varying version of the shorter wavelength disturbance. Thus the longer wavelength disturbance was due to interference at the outer wall between different radial harmonics.

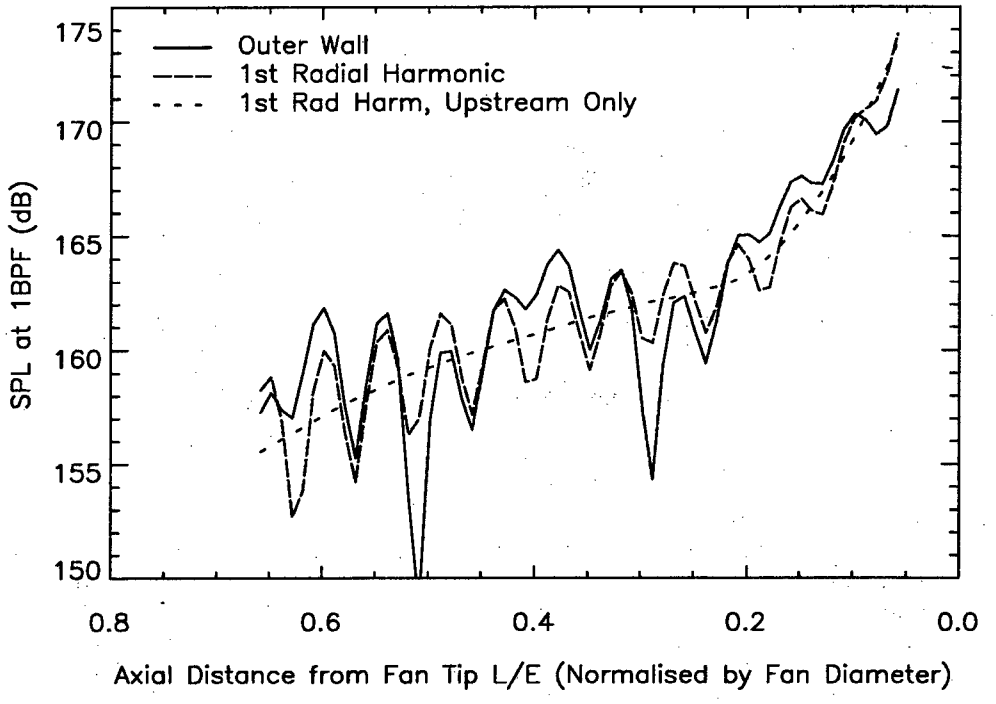

Figure 2. Steady CFD for Rotor Alone Noise, Bessel-Fourier Decomposition and Wavesplitting

In some cases this level of analysis is sufficient. The radial harmonic breakdown along the duct gives a great deal of information about both the source amplitude and the accuracy of the code, as will be discussed later. In this case, however, a further step is necessary to isolate the cause of the short wavelength oscillations. The periodic nature of the oscillations suggests some form of standing wave, and this particular case was run with 1D non-reflecting boundary conditions at the inlet boundary, which are known to be poor for the wavelengths and frequencies of interest.

By decomposing the axial velocity also into Bessel-Fourier harmonics the pressure variation represented by the long dashes in fig 2 can be split into forward and backward travelling components. The short dashes in that figure represent the upstream travelling component. The result is a smooth line, demonstrating that the oscillations observed at the outer wall are indeed due to the presence of a downstream wave reflected from the inlet boundary.

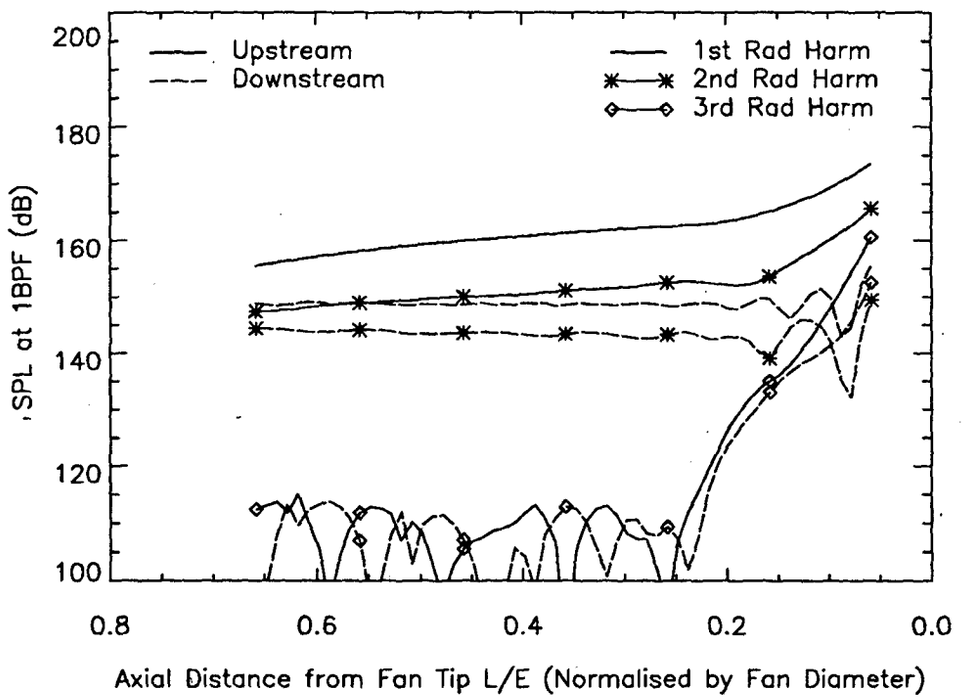

Figure 3. Steady CFD for Rotor Alone Noise: First Three Radial Harmonics of Upstream and Downstream Waves

Figure 3 shows upstream and downstream wave components of the noise for the first three radial harmonics at the first blade passing frequency. The third harmonic is cut-off and will be discussed later. The first two harmonics are cut-on, and Tyler and Sofrin's linear method would predict propagation at constant amplitude. The upstream waves, however, decay considerably, especially in the vicinity of the fan. Fig 4 shows the first radial harmonic, compared with Morfey and Fisher's 1D non-linear decay theory (Morfey and Fisher 1970). The agreement is not expected to be exact, given the assumptions implicit in the 1D calculation. However, the relatively close agreement near the fan suggests that the decay is in the main genuine and due to non-linear effects. The less good agreement further from the fan is thought to be due to the increasingly coarse grid away from the fan, which has the effect of attenuating the higher circumferential harmonics.

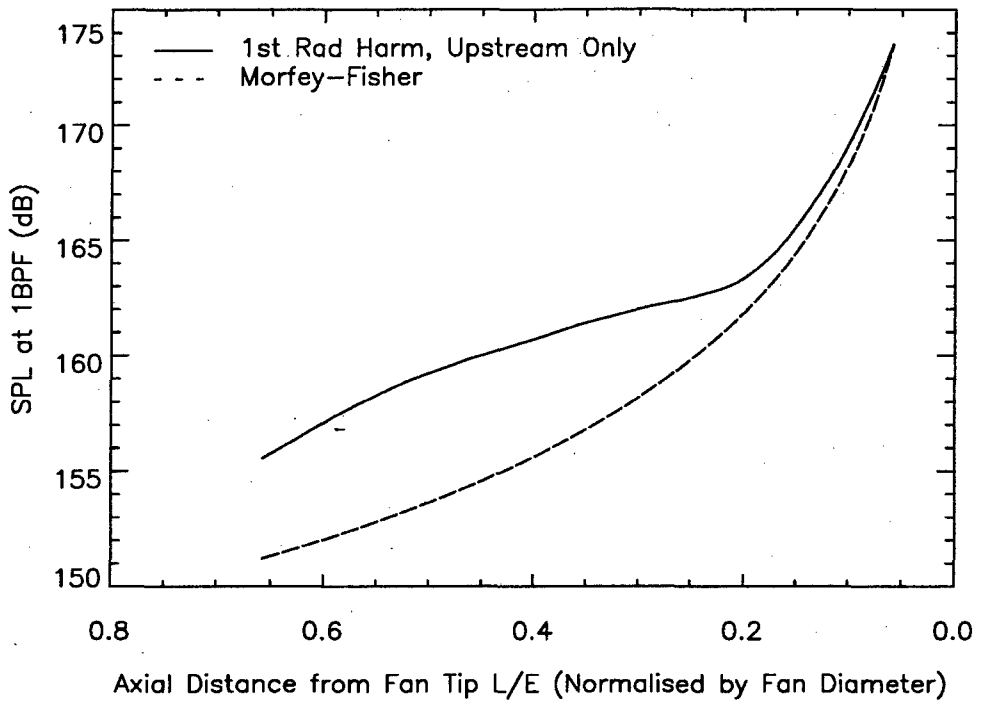

Figure 4. Steady CFD for Rotor Alone Noise, Comparison of First Radial Harmonic with Morfey-Fisher 1D Non-linear Decay Theory

The downstream travelling waves (dashed lines in fig 3) are lower amplitude and are less affected by non-linear decay. Hence they travel at more nearly constant amplitude over the majority of the domain. The high ratio of reflected to incident amplitude at the inlet to the domain confirms that the boundary conditions are indeed behaving poorly. The upstream wave amplitude, however, allows a quantitative noise estimate to be obtained without contamination from these reflected waves, provided that the response of the fan to the downstream waves can be ignored. In this particular case the non-linear decay is sufficient to mask any minor changes in source amplitude, and the result is unlikely to be affected by the presence of the reflected waves.

The oscillations in amplitude of the reflected waves near the fan leading edge are a result of the assumptions in the mathematics of the wavesplitting. The relationship between pressure and velocity as calculated by the CFD code are slightly different to the analytic values, due to discretisation effects and the assumptions inherent in the analysis. Hence there is a limit to the extent to which upstream and downstream waves can be discriminated. This can be a particular problem near the cut-off boundary, as explained under example 2. The results in figure 3 show that upstream and downstream waves of this type can be discriminated to within 15-20dB of the higher signal amplitude.

The third harmonic shown in figure 3 is cut-off, and decays rapidly with axial distance to a 'floor' level of around 110dB. This floor level is set by 'leakage' between radial harmonics. The actual propagating modes in the calculation are not pure Bessel-Fourier harmonics, both because of discretisation effects and because the mean flow is not uniform. Hence the Bessel-Fourier breakdown in the wavesplitting process calculates some content at all radial harmonics even if only one mode is present. Nonetheless, the discrimination between radial modes (over 40dB from the first harmonic amplitude to the 'floor' level in fig 3) is more than sufficient for most purposes.

The reason for the poor discrimination between upstream and downstream waves near the domain exit at this third harmonic is not known. Typically (away from the cut-off point itself) reasonable discrimination is obtained for both cut-on and cut-off waves.

Figure 5 shows the amplitude of the upstream component of the third harmonic compares well with the exponential decay predicted in Tyler and Sofrin's theory.

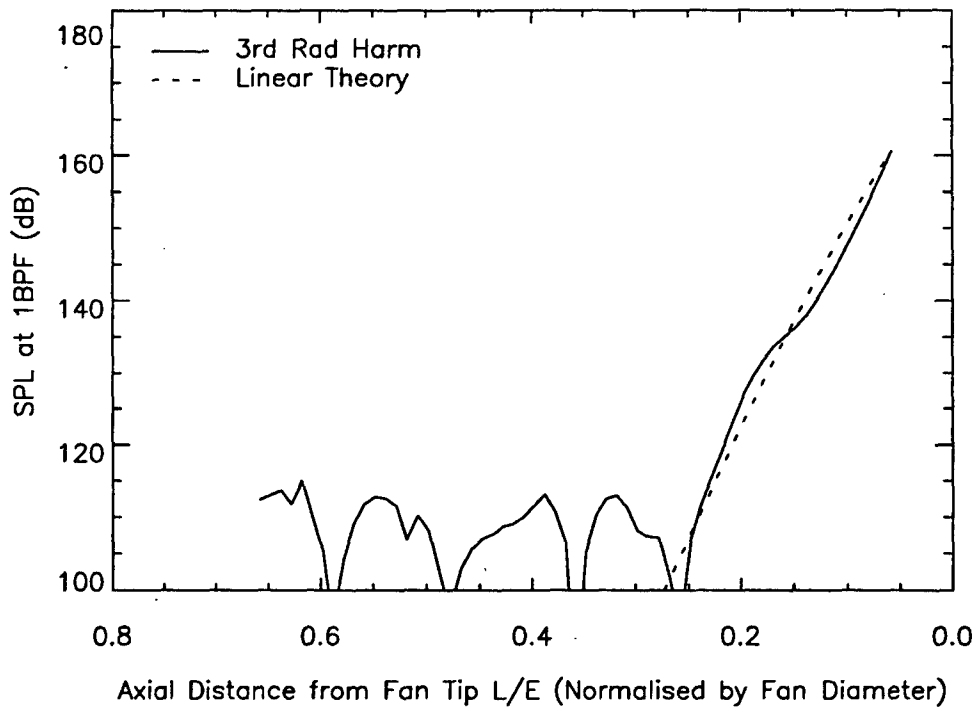

Figure 5. Steady CFD for Rotor Alone Noise, Comparison of Third Radial Harmonic Upstream Travelling Wave with Linear Theory

The noise output of the fan can only be estimated in the region where the mesh is sufficiently fine. In this case, the noise output (fig 3) is 163dB SPL in the first radial harmonic, 152dB in the second, and negligible output in the third and higher harmonics, all at a position 0.2 diameters upstream of the fan. Note that this figure could not easily have been obtained from either the wall pressure or the harmonic breakdown of pressure alone (fig 2).

Figure 4 suggests that there is still significant non-linear behaviour upstream of the 0.2m point. Depending on the use to which the data is to be put, it may be important to contain the non-linear behaviour within the CFD domain. In this case a second CFD calculation would be required with increased mesh density in the upstream region.

To summarise, in this first example the wavesplitting method has been used

- to demonstrate that the observed oscillations in pressure are due to reflections from the inlet boundary and interference between radial harmonics,
- to match the behaviour of the CFD solution to expectation and hence to give confidence in the solution,
- to gauge the significance of non-linear effects, and
- to obtain a quantitative measure of the fan-forward rotor alone noise in the presence of significant reflections from the upstream plane.

Method

The post-processing required for the wavesplitting method can be broken down into the following steps:

1. Fourier transform in time (non-linear unsteady CFD codes only).
2. Interpolate onto axial planes.
3. Decompose into Bessel-Fourier harmonics.
4. Calculate linear propagation parameters at each axial plane based on average mean flow.
5. Use linear theory to split Bessel-Fourier harmonics into upstream and downstream components.

It can be useful, in comparing the relative strengths of the radial harmonics, to add a sixth step:

6. Calculate acoustic energy flux for upstream and downstream components.

In linear theory with uniform axial mean flow and parallel annulus ducts (Tyler and Sofrin 1961), cut-on modes propagate with uniform amplitude and cut-off modes with exponential decay. Both types propagate with phase varying linearly with axial distance. The decay rates and axial wavenumber are calculated at step 4, and so by plotting amplitude on a log scale (eg as SPL) and phase on a linear scale, it is easy to compare the modal behaviour with theory. Variations from linear behaviour can then be easily identified and subjected to further analysis, as demonstrated in the examples above and below.

Step 1. Fourier transform in time.

Both the theoretical linear calculations and the wavesplitting require data at fixed position and fixed frequency. In steady CFD calculations on rotor blades the frequency is fixed by the circumferential harmonic (that is, a first blade passing harmonic in the circumferential direction will be heard at first blade passing frequency by a stationary observer). In linear unsteady calculations the frequency is fixed in the frame of reference of the CFD domain, and again the frequency in the stationary domain can be easily calculated for a given circumferential harmonic. In non-linear calculations a Fourier transform in time is required first to obtain data at a given frequency. Such a transform is easily calculated given a periodic converged solution.

Step 2. Interpolate onto axial planes.

Some care is required in this step, particularly in the presence of shocks, where a simple linear interpolation can lead to shock smoothing. In cases with structured or semi-structured grids, greater accuracy can sometimes be obtained by applying a circumferential FFT first (that is, to bring the first part of step 3 forward), and then to interpolate axially for amplitude and phase at a given plane.

Step 3. Decompose into Bessel-Fourier harmonics.

This process consists of a Fourier transform circumferentially, followed by a Bessel function decomposition in the radial direction. The latter is aided by the orthogonality condition (appendix 1). The choice of flow variables to be decomposed depends on the type of wavesplitting technique to be employed, as described under step 5.

Step 4. Calculate linear propagation parameters at each axial plane based on average mean flow.

The linear propagation parameters (axial wavenumbers for upstream and downstream propagating waves) are calculated for each circumferential and radial harmonic, based on a duct with parallel annulus walls and uniform axial mean flow (appendix 1). Given the approximations of the method a simply calculated Mach number based on area average axial velocity and temperature (or equivalent) at each axial plane is sufficient to define the equivalent mean flow.

Step 5. Use linear theory to split Bessel-Fourier harmonics into upstream and downstream components.

This step is not always necessary. In particular if the boundary conditions in the CFD calculation are known to be genuinely non-reflective, and the duct in which the analysis is being performed is fairly uniform, then the noise can be assumed to be travelling in a single direction only, and the pressure information alone is sufficient. In many cases, however, the effect of the boundary conditions and duct geometry is not known at acoustic wavelengths and frequencies, and this step is required.

Two methods of performing the wavesplit are detailed in appendix 1. The first, simpler method uses just the pressure and the axial velocity from the CFD solution, and is based on the assumption of irrotational flow (that is in total, not just irrotational mean flow). This is often a good approximation in the inlet duct. It is unlikely to be sufficient in the OGV exit duct, or in other calculations where vortical waves are prominent in the flow solution. Boundary conditions too (even if termed non-reflective) can introduce vorticity at the inlet plane.

The second method is still based on the assumption of uniform axial mean flow, but allows for vortical waves in the solution. This method is more complex, using the divergence of the flowfield to remove the effects of vorticity.

Step 6. Calculate acoustic energy flux for upstream and downstream components.

Usually the most useful quantitative output from the analysis method is the noise amplitude (SPL) in the different circumferential and radial harmonics. Sometimes, however, it is useful to compare the noise generated in the different harmonics, or to combine the results into a single figure. Tester (1972) gives a formula (reproduced in appendix 1) for acoustic energy flux based on the same uniform axial flow and parallel duct assumptions as the theoretical calculations in step 4 and the irrotationality assumption of the first method in step 5. The calculation can be applied directly to the interpolated flow variables at each axial plane at step 2, but it can also be applied to the upstream and downstream components of the individual circumferential and radial harmonics. Under the given assumptions these behave independently for cut-on modes (that is, the total energy flux is the sum of the constituents). For cut-off modes energy is

transported by combinations of upstream and downstream propagating waves, and thus the calculation has to be performed prior to the wavesplit.
By summing the energy flux over all the modes in one direction only (upstream or downstream), it is possible to calculate an overall source level in the cut-on modes disregarding any waves reflected from the boundary of the CFD domain.

Example 2: Unsteady CFD, Boundary Conditions, Dissipation Errors

This example comes from an investigation into non-reflective boundary conditions. Two separate 3D unsteady linear calculations were performed in a parallel annulus duct with two types of boundary condition at the inlet (Giles type 1D and 2D non-reflecting, Giles 1990, Saxer and Giles 1993). A uniform rectangular grid was used, with 61 points axially and 41 points circumferentially and radially, representative of a short section of the inlet duct for a typical aeroengine fan at rig-scale (Outer diameter around 0.43m). The base flow for the linear calculation was set to be uniform axial flow, again representative of a fan inlet duct at transonic conditions. In each case a 26-lobed upstream travelling acoustic wave was input at the outflow boundary, and the output analysed using the method described in the previous section.
Figure 6 shows some of the results from the calculation with 1D non-reflecting boundary conditions. The input wave had constant amplitude radially. This implies content at all radial harmonics, and so it is unsurprising that the wall amplitude (solid line in Figure 6) varies considerably along the length of the duct. The total amplitude of the first radial harmonic (dashed line) also varies, due to reflections from the inlet boundary. When the wavesplitting process is applied using the static pressure and axial velocity (dotted line), the long lengthscale oscillations are removed, but more oscillations are present at a shorter lengthscale.
The oscillations in wave amplitude are the result of vorticity introduced by the boundary conditions at the inlet boundary. The reflected vortical waves interfere with the axial velocity field, preventing an accurate analysis of the acoustic waves. This effect can be removed by applying the wavesplit method using static pressure and the divergence of the velocity field (see appendix 1). The result of this analysis is shown as the dash-dot line in Figure 6. All oscillations have been removed, leaving a uniformly decaying amplitude from which a quantitative estimate can be made of the dissipation error inherent in the numerical calculation (15dB per duct diameter). Similar calculations could be performed using the phase of individual waves to determine the propagation phase error.

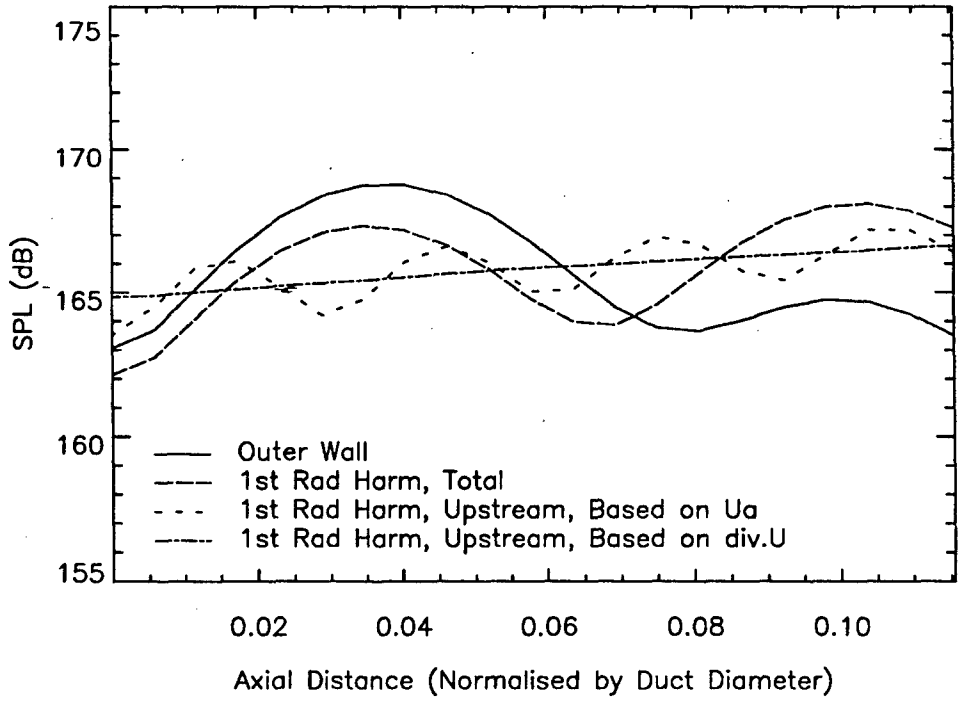

Figure 6. Unsteady CFD, Wavesplit Based on Ua and div.U

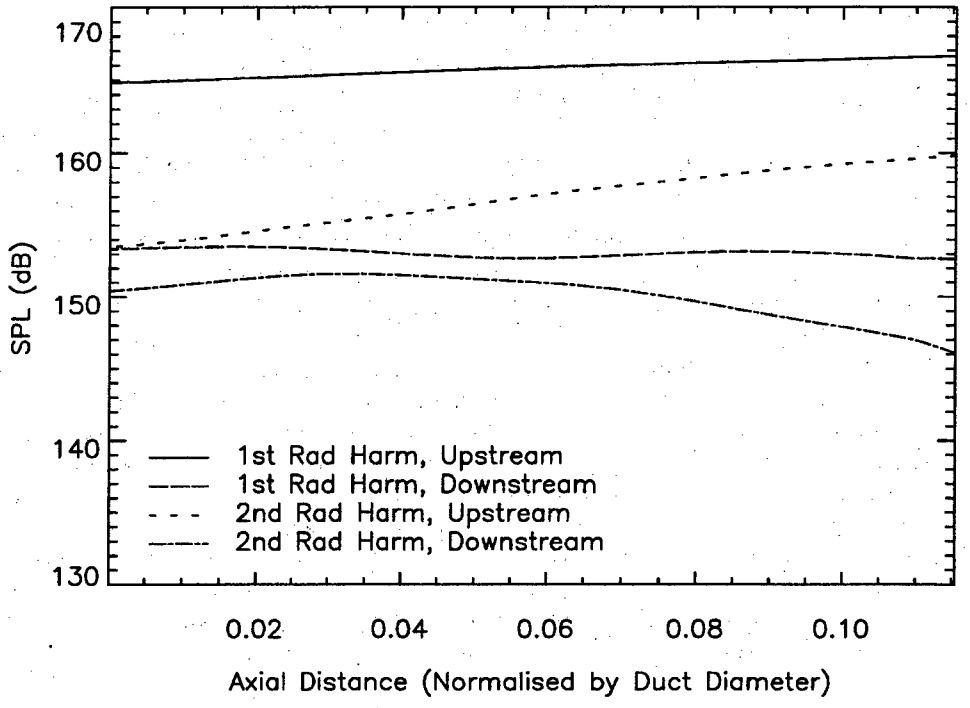

Figure 7. Unsteady CFD: Upstream and Downstream Waves

Full results from the wavesplitting procedure at the first and second radial harmonics are presented in Figure 7. The second harmonic is very close to cut-off (cut-off ratio 1.01), and illustrates some of the difficulties commonly encountered close to the cut-on/cut-off boundary. The upstream wave shows an exceptionally fast rate of decay with axial distance, and the downstream wave in particular shows significant non-linear behaviour, in that the (log) amplitude varies non-linearly with axial distance.

Because information in near cut-off modes travels slowly along the duct there is more time for genuine non-linear and viscous phenomena to affect noise propagation between axial planes. The present calculations, however, were performed with an inviscid linear code, and so neither of these factors can explain the high decay rate of the upstream wave. The decay here is a result of the numerical smoothing applied in the CFD code.

In a CFD calculation smoothing is balanced by the rate at which the wave information travels upstream. Hence waves near cut-off tend to be heavily attenuated. The principle can illustrated using a simplistic 2D wave equation solved analytically with second order smoothing on the pressure term. Using the nomenclature defined in the appendix,

$$\frac{\partial \mathbf{u}}{\partial t} = -c\nabla p$$

$$\frac{\partial p}{\partial t} = -c\nabla.\mathbf{u} + \varepsilon\nabla^2 p$$

The level of smoothing ε is assumed to be small and fixed independently of the frequencies and wavelengths present in the solution. For a cut-on upstream plane wave at a given frequency ω it is possible to show (with some algebra) that to first order in ε the axial wavenumber of the smoothed wave is

$$\lambda = \hat{\lambda} + i\varepsilon\omega^2/2c^2u_{inf}$$

where $u_{inf} = -c^2\hat{\lambda}/\omega$ is the rate at which information travels upstream, and $\hat{\lambda}$ is the axial wavenumber in the absence of smoothing. Thus the rate of decay with axial distance (determined by the imaginary part of the axial wavenumber) is $\varepsilon\omega^2/2c^2u_{inf}$. Hence waves near the cut-off boundary ($u_{inf} \to 0$) are heavily attenuated.

In addition to the greater non-linear and smoothing effects, the wavesplitting process itself is liable to errors close to the cut-on/cut-off boundary. At this boundary the upstream and downstream linear waves

coalesce. In theory this could give large numerical errors in the wavesplitting solution (mathematically, f^{us} and f^{ds} get very close in equations 18, 19 of the appendix)[2]. In practice this is rarely a problem: even with a cut-off ratio of 1.01 there is sufficient discrimination to prevent large numerical errors.

Of much greater significance is the fact that the discrepancies between the CFD calculated modes and the analytical modes grow large near the cut-on/cut-off boundary. In the analytic axial mean flow formulation the axial wavenumber λ becomes very sensitive to flow conditions, and in particular to the cut-off ratio $\xi = \omega/c\mu\left(1-U^2\right)$. Indeed, it can be seen from equation 7 of the appendix that at the boundary itself the derivative of λ with respect to ξ becomes infinite. It is unsurprising therefore that the analytic modes and those calculated by CFD (with non-uniform mean flow, smoothing and discretisation errors) can be very different near the boundary.

The following graph illustrates the problems that can occur near the cut-off boundary. The simple case is taken of a 2D wave equation solved using analytic derivatives in time and axially (x direction), but a simple central difference numerical derivative in the y direction. Forty points per wavelength were used, which is usually sufficient to give reasonable wave propagation. An exact modal solution to the numerical problem was calculated for a range of frequencies, to which the wavesplitting technique was applied. The graph shows the amplitude of the forward and reverse waves calculated by the method for points close to the cut-off boundary. As expected, the errors grow large close to the boundary, and very close to the boundary the calculated waves in both directions can be much larger in amplitude than the genuine wave. Note, though, that the errors are highly concentrated in the region of the boundary: away from this point (towards either cut-on or cut-off) the errors are small and the wavesplitting technique is successful.

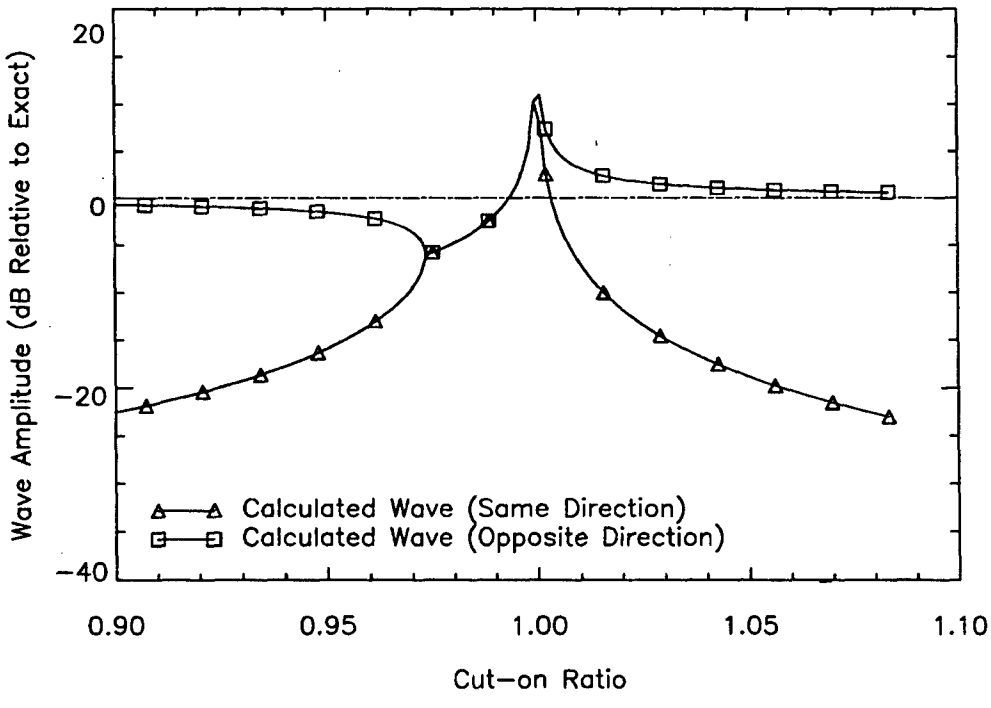

Figure 8. Errors in Wavesplitting Method Close to the Cut-Off Boundary

[2] With the second wavesplitting method, based on pressure and the divergence of the velocity, numerical errors could also cause a problem in regions of low or zero mean flow. This is because, although the axial wavenumbers of the upstream and downstream waves remain discrete with decreasing mean flow, the wavesplitting parameters f^{us} and f^{ds} (equation 22 of the appendix) become identical.

Returning to the CFD example, Figure 9 shows the results of the wavesplitting analysis for the 1D and 2D non-reflective boundary conditions. The 1D boundary conditions give a reflected wave with amplitude 11.5dB lower than the incident. The second radial harmonic, however, shows a reflection only 3dB lower than the incident (accepting the errors discussed above in the wavesplitting for this harmonic). Care has to be applied here, in that boundary conditions can scatter an incident wave at one radial harmonic into reflected waves at other harmonics. However, a more detailed analysis of the 1D non-reflective boundary conditions used in this case has shown that the downstream wave at the second radial harmonic is indeed a reflection of the same harmonic, rather than a scattered reflection from the first harmonic. The 2D non-reflective boundary conditions give a reflection of the first harmonic 30dB lower than the incident. This level is close to the level at which forward and backward waves can be discriminated, hence the oscillation with axial distance. The second harmonic is reflected at a level 4dB lower than the incident. A more detailed analysis of the boundary conditions has shown that this value would be 7.6dB without scattering from the higher amplitude first radial harmonic.
In both cases the high reflection coefficients for the second harmonic mirror the difficulty in wavesplitting close to the cut-off boundary.

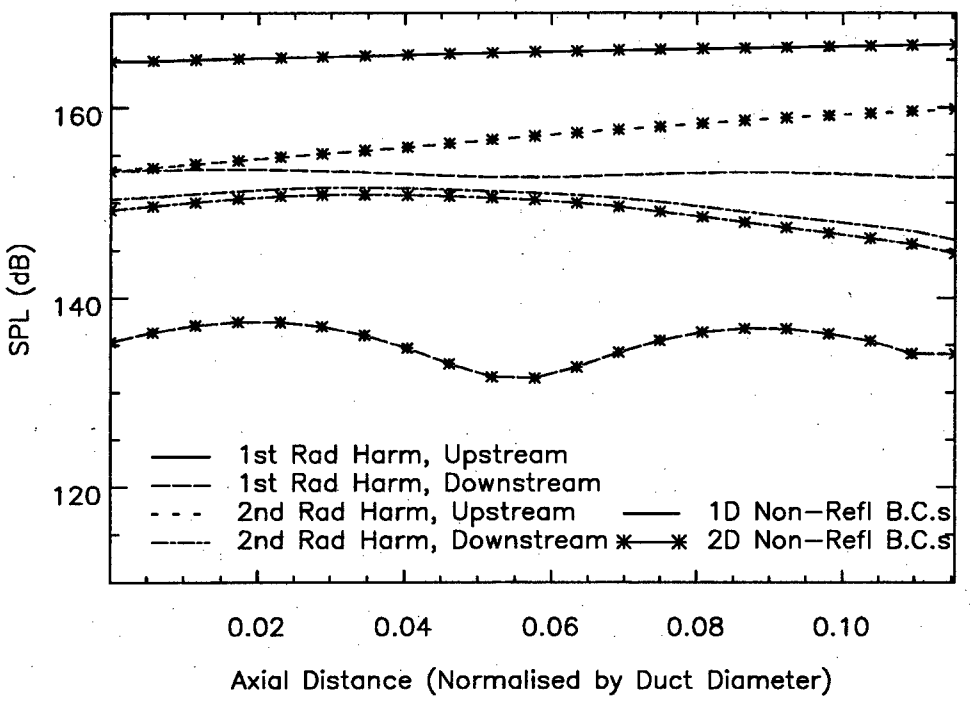

Figure 9. Unsteady CFD: Comparison of 1D and 2D Boundary Conditions

Further Example

The wavesplitting method has been applied to a flat plate wake/vane interaction case (Wilson 2001). In that work the method was also extended to provide fully 3D non-reflecting boundary conditions at inflow and exit.

Limitations

The major limitations of the analysis procedure have been identified as follows:

1) The method as it stands is unsuitable for use in regions where the propagating modes are known to differ strongly from Tyler and Sofrin modes. Examples are:
   a) Fan exit, where the high degree of swirl significantly affects the propagating modes.
   b) Lined ducts (although the method can still be applied in any hardwall regions upstream and downstream of the liner).
2) The method gives poor results close to the cut-on/cut-off boundary (as discussed under example 2).

3) The wavesplitting method based on pressure and axial velocity is limited to regions of irrotational flow. This can be a good approximation in the fan inlet region, subject to the boundary conditions at the inlet plane producing negligible vorticity. This limitation can be overcome by using the second wavesplitting method, based on pressure and the divergence of the velocity.

Summary

A procedure has been developed for deriving tone noise information from CFD solutions in the fan stage. A wavesplitting method is used at a number of axial locations upstream of the fan to derive upstream and downstream wave information from the CFD calculated flowfield. The development of these waves with axial distance is then compared to well-understood linear behaviour.

The method is equally applicable to the bypass duct downstream of the outlet guide vane (where, like the inlet, the mean flow is approximately axial). Application to other areas is subject to the limitations outlined in the previous section.

Examples have been given of how the method can be used

- to identify regions of non-linear behaviour
- to identify and eliminate the effect of modest spurious reflections at the domain boundaries
- to identify and eliminate the effect of modest vortical waves present in the solution
- to quantify numerical dissipation errors

and hence

- to quantify tone noise generation.

References

Giles MB, 1990, *Non-Reflecting Boundary Conditions for Euler Equation Calculations*, AIAA Journal, Vol 28, No. 12, pp 2050-2058

Cantrell RH, and Hart RW, 1964, *Interaction between Sound and Flow in Acoustic Cavities: Mass, Momentum and Energy Considerations*, J.A.S.A. Vol 36, No. 4, pp697-706

Morfey CL and Fisher MJ, 1970, *Shock-Wave Radiation from a Supersonic Ducted Rotor*, J. Roy. Aeron. Soc., vol 74, pp579-585

Rowley CW and Colonius T, 1998, *Numerically Nonreflecting Boundary Conditions for Multidimensional Aeroacoustic Computations*, AIAA 98-2220, presented at 4th AIAA/CEAS Aeroacoustics Conference, Toulouse, June 2-4

Saxer AP, and Giles MB, 1993, *Quasi-Three-Dimensional Nonreflecting Boundary Conditions for Euler Equations Calculations*, Journal of Propulsion and Power, March-April (No. 2), pp263-271

Tester BJ, 1972, *Sound Attenuation in Lined Ducts Containing Subsonic Mean Flows*, PhD Thesis, Univ. Southampton,

Tyler JM and Sofrin TG, 1962, *Axial Flow Compressor Noise Studies*, Trans S.A.E., Vol 70, pp309-332

Wilson AG, 2001, *Application of CFD to Wake/Aerofoil Interaction Noise – A Flat Plate Validation Case*, AIAA-2001-2135, presented at 7th AIAA/CEAS Aeroacoustics Conference, Maastricht, 28-30 May

Appendix 1 – Mathematics of Wavesplitting Technique

Nomenclature

U	Mean flow speed (assumed axial) normalised by speed of sound
$\bar{p}$	Mean flow pressure
$\bar{\rho}$	Mean flow density
c	Speed of sound based on mean flow pressure and density
u	Perturbation velocity normalised by speed of sound
p	Perturbation pressure, normalised by $\gamma\bar{p}$
γ	Ratio of specific heats (assumed constant)

Wave Solutions of the Euler Equations in Parallel Annulus Ducts

The linearised Euler equations for a perfect gas with constant ratio of specific heats and uniform mean flow in the x direction can be expressed as

$$\frac{1}{c}\frac{\partial \mathbf{u}}{\partial t} + U\frac{\partial \mathbf{u}}{\partial x} = -\nabla p \qquad (1)$$

$$\frac{1}{c}\frac{\partial \rho}{\partial t} + U\frac{\partial \rho}{\partial x} = -\nabla.\mathbf{u} \qquad (2)$$

Together with the equation of state and the energy equation this represents five equations in five unknowns. The wave solutions (that is, solutions for the flow variables that preserve their shape axially) are well known, and correspond to two acoustic waves, two vorticity waves and a single entropy wave.

For a parallel wall annular duct the acoustic waves can be written as

$$\mathbf{u} = \nabla\phi \qquad (3)$$

$$\phi = ip/(\omega/c - U\lambda) \qquad (4)$$

where $p = p_{m.k.\omega}\exp i(\omega t - \lambda x - m\theta)B_m^k(r)$ (5)

and $B_m^k(r)$ is a combination of the J- and Y-type Bessel functions:

$$B_m^k(r) = aJ_m(\mu_m^k r) + bY_m(\mu_m^k r), \qquad (6)$$

where a, b and μ_m^k are chosen to satisfy the boundary condition $\mathbf{u}_r = \frac{\partial\phi}{\partial r} = 0$ on both the inner and outer walls. If no routine is available to give these functions, a method is outlined later which requires only evaluation of the individual Bessel functions.

For each circumferential harmonic m and radial harmonic k there are two possible axial wavenumbers λ defined by

$$\lambda = \frac{-U\,\omega/c \pm \sqrt{(\omega/c)^2 - \mu_m^{k\,2}(1-U^2)}}{1-U^2} \qquad (7)$$

λ is either real or complex depending on the sign of the term under the square root. It is convenient to consider the two cases separately:

Cut-on waves (λ real)

It can be seen from equation 5 that if λ is real, then the wave propagates axially at constant amplitude and varying phase. For forward subsonic mean flow $0 < U < 1$, the negative root in equation 7 corresponds to an upstream travelling wave, whilst the positive root corresponds to a downstream wave. Note that with mean flow $U > 0$ it is possible for λ to remain negative even for the downstream travelling wave. In this

case the wavefront is angled in the same direction as the upstream wave and indeed appears to move upstream. The group velocity, however, defining the direction in which information is transported, is still downstream, as is the transport of energy.

Cut-off waves (λ complex)

If λ is complex, then the wave decays exponentially in the direction of propagation. For forward subsonic mean flow $0 < U < 1$, the root of equation 7 with positive imaginary part represents an upstream wave decaying with upstream distance, and the root with negative imaginary part represents a downstream wave decaying with downstream distance. The phase variation is fixed by the first term in equation 7, which is independent of m and k. Hence all cut-off waves have the same 'spiral angle' (that is, the same rate of change of phase with axial distance).

In each case, the two roots of equation 7 correspond to one upstream and one downstream wave. Entropy and vorticity waves make no contribution to the pressure, and so at a given frequency ω, circumferential mode m and radial harmonic k, the entire unsteady pressure field can be written as the sum of the contributions from the two acoustic waves:

$$p = \left[p^{us}(x) + p^{ds}(x)\right]\exp i(\omega t - m\theta)B_m^k(r), \text{ where} \qquad (8)$$

$$p^{us} = cst.\exp\left(-i\lambda^{us}x\right)$$
$$p^{ds} = cst.\exp\left(-i\lambda^{ds}x\right) \qquad (9, 10)$$

Thus if p^{us} and p^{ds} are known at any single axial plane, then their (theoretical) values can be calculated at any other plane. Two methods are given below for splitting the unsteady pressure into its upstream and downstream components, depending on whether or not the flow can be assumed irrotational.

Wavesplitting in Irrotational Flow

The velocity and pressure perturbations of individual acoustic waves are linked by equations 3 and 4. Entropy waves, furthermore, make no contribution to either pressure or velocity. Hence for each harmonic (ω, m, k) the axial velocity can be derived from the upstream and downstream components of pressure (equ 8) as follows:

$$u_x = \left[u_x^{us}(x) + u_x^{ds}(x)\right]\exp i(\omega t - m\theta)B_m^k(r), \text{ where} \qquad (11)$$

$$u_x^{us} = f^{us}p^{us}$$
$$u_x^{ds} = f^{ds}p^{ds}$$
$$f^{us} = \lambda^{us}/\left(\omega/c - U\lambda^{us}\right)$$
$$f^{ds} = \lambda^{ds}/\left(\omega/c - U\lambda^{ds}\right) \qquad (12, 13, 14, 15)$$

Of more interest is the inverse process, whereby the upstream and downstream components can be determined from the static pressure and axial velocity. If at a given axial plane and these two variables are decomposed into Bessel-Fourier harmonics, with coefficients p', u', then

$$p' = p^{us} + p^{ds}$$
$$u_x' = u_x^{us} + u_x^{ds} = f^{us}p^{us} + f^{ds}p^{ds} \qquad (16, 17)$$

Hence

$$p^{us} = \left(f^{ds}p' - u_x'\right)/\left(f^{ds} - f^{us}\right)$$
$$p^{ds} = \left(f^{us}p' - u_x'\right)/\left(f^{us} - f^{ds}\right) \qquad (18, 19)$$

Wavesplitting in the Presence of Vortical Waves

In the presence of vortical waves the previous wavesplitting method fails, because the axial velocity is no longer a function of the acoustic waves alone. Hence another method is presented here, based on pressure and the divergence of the velocity field ($\nabla \cdot \mathbf{u}$). Note that this method too is based on the assumption of a uniform axial mean flow. Thus, whilst small amounts of vorticity can be handled using this method, it is not suitable for highly vortical flows such as those found between an aeroengine fan rotor and outlet guide vane.

The divergence of the velocity for acoustic waves can be calculated from the two pressure coefficients (equs 9, 10) using equ 4;

$$\begin{aligned}\nabla \cdot \mathbf{u}^{us} &= \nabla^2 \phi^{us} \\ &= -\left(\lambda^{us\,2} + \mu_m^{k\,2}\right)\phi^{us} \\ &= -\left(\lambda^{us\,2} + \mu_m^{k\,2}\right) ip^{us} / \left(\omega/c - U\lambda^{us}\right) \\ &= f^{us} p^{us}\end{aligned} \qquad (20)$$

where $f^{us} = -i\left(\lambda^{us\,2} + \mu_m^{k\,2}\right) / \left(\omega/c - U\lambda^{us}\right)$. (21)

With some manipulation, this can be reduced to

$$f^{us} = -i\left(\omega/c - U\lambda^{us}\right), \qquad (22)$$

and similarly for the downstream waves.

Both $\nabla \cdot \mathbf{u}$ and p are identically zero for vorticity and entropy waves. Hence the upstream and downstream components can be obtained from $\nabla \cdot \mathbf{u}$ and p in an identical manner to the irrotational case (equs 16 to 19), but with $\nabla \cdot \mathbf{u}$ instead of u_x, and the new definitions of f^{us}, f^{ds}.

$\nabla \cdot \mathbf{u}$ can be calculated directly from the CFD solution using a simple difference sum. A refinement is to use the flow equations (1, 2) to remove the axial derivative of the velocity, such that the wavesplit can be performed using only data from a single axial plane. The following analysis is for isentropic flow, although the result also holds in the presence of entropy waves.

For isentropic flow, given the normalisation used, the continuity equation (2) can be expressed in terms of pressure:

$$\frac{1}{c}\frac{\partial p}{\partial t} + U\frac{\partial p}{\partial x} = -\nabla.\mathbf{u} = -\overset{2D}{\nabla}.\mathbf{u} - \frac{\partial u_x}{\partial x}, \qquad (23)$$

where $\overset{2D}{\nabla}.\mathbf{u} = \frac{1}{r}\frac{\partial (r u_r)}{\partial r} + \frac{1}{r}\frac{\partial u_\theta}{\partial \theta}$. (24)

But from the axial component of the momentum equation (1),

$$\frac{\partial p}{\partial x} = -\frac{1}{c}\frac{\partial u_x}{\partial t} - U\frac{\partial u_x}{\partial x} \qquad (25)$$

Substituting this into equ 23, and applying a transform in the time direction $\frac{\partial}{\partial t} \rightarrow iw$,

$$\frac{iw}{c}p + U\left(-\frac{iw}{c}u_x - U\frac{\partial u_x}{\partial x}\right) = -\overset{2D}{\nabla}.\mathbf{u} - \frac{\partial u_x}{\partial x}$$

$$\Rightarrow \frac{\partial u_x}{\partial x} = -\left(\overset{2D}{\nabla}.\mathbf{u} + \frac{iw}{c}(p - Uu_x)\right)\Big/\left(1 - U^2\right) \qquad (26)$$

$$\Rightarrow \nabla.\mathbf{u} = \overset{2D}{\nabla}.\mathbf{u} + \frac{\partial u_x}{\partial x} = -\left(U^2\overset{2D}{\nabla}.\mathbf{u} + \frac{iw}{c}(p - Uu_x)\right)\Big/\left(1 - U^2\right)$$

Thus to calculate $\nabla \cdot \mathbf{u}$ from data at a single axial location, it is necessary only to calculate the radial and circumferential derivatives in equ 24 and to substitute the result together with values for p and u_x into the equation above. Note that the circumferential derivative is trivial, as the data has previously been Fourier transformed. In the radial direction a simple finite difference method is often sufficient.

The use of a simple finite difference sum and the inclusion of the analytic flow equations do make the method somewhat approximate. Nonetheless, provided the vortical waves are of similar amplitude to the acoustic waves (or smaller) it is effective in isolating the acoustic component, as illustrated by example 2 of the main paper.

Acoustic Energy Flux

Tester (1972) gives an equation for modal energy flux with uniform axial mean flow (based on that of Cantrell and Hart, 1964). In the current nomenclature, at any given frequency,

$$I_{xmk} = \frac{\bar{\rho}c^3 B_{mk}^2}{2}\mathrm{Re}\left\{p_{mk}u_{mk}^* + M_x p_{mk}p_{mk}^* + M_x^2 p_{mk}u_{mk}^* + u_{mk}u_{mk}^* M_x\right\} \qquad (27)$$

where p_{mk} and u_{mk} represent coefficients of pressure and axial velocity at a single circumferential (m) and radial (k) harmonic at the given frequency. The term

$$B_{mk}^2 = \int B_m^k(r)^2 .2\pi r\mathrm{d}r \qquad (28)$$

has been added to integrate the energy flux over the area of the duct (note that $B_{mk}^2 = \int B_m^k(r)^2 .2\pi r\mathrm{d}r$ is purely real in this equation).

If the (m,k) mode is cut-on, then the upstream and downstream travelling waves are orthogonal with respect to the above equation. That is, the total energy flux in the mode is the sum of that calculated from just the upstream and downstream travelling components. If the mode is cut-off, then the upstream and downstream travelling waves interact to give energy flux, and the calculation has to be performed prior to the wavesplit.

Given the orthogonality of the radial harmonics, the total acoustic energy flux in a given circumferential harmonic m can also be calculated by integrating the radial profiles directly:

$$I_{xm} = \frac{\bar{\rho}c^3}{2}\int \mathrm{Re}\left\{p_m u_m^* + M_x p_m p_m^* + M_x^2 p_m u_m^* + u_m u_m^* M_x\right\}2\pi r\mathrm{d}r \qquad (29)$$

where p_m and u_m now represent radial profiles of pressure and axial velocity components at the mth circumferential harmonic. Provided that a single value of M_x is used (rather than a radial profile) the result is equal to the sum of equ 27 over all radial harmonics k.

Calculation of $B_m^k(r)$

If no routine is available to give these functions, a method is outlined here which requires only values of the Bessel functions themselves and a method of hunting for zeros.

The boundary conditions require

$$\frac{\partial B_m^k}{\partial r} = a\mu_m^k J_m'(\mu_m^k r) + b\mu_m^k Y_m'(\mu_m^k r) = 0 \text{ at } r = r_1, r_2$$
$$\Rightarrow \quad aJ_m'(\mu_m^k r_1) + bY_m'(\mu_m^k r_1) = 0$$
$$aJ_m'(\mu_m^k r_2) + bY_m'(\mu_m^k r_2) = 0 \qquad (30, 31, 32)$$

This only has non-zero solutions for a, b if

$$J_m'(\mu_m^k r_1)Y_m'(\mu_m^k r_2) = Y_m'(\mu_m^k r_1)J_m'(\mu_m^k r_2). \qquad (33)$$

Using the recurrence relationships

$$2J_m'(z) = J_{m-1}(z) - J_{m+1}(z) \text{ and } 2Y_m'(z) = Y_{m-1}(z) - Y_{m+1}(z) \qquad (34, 35)$$

this equation can be rewritten

$$\left(J_{m-1}(\mu_m^k r_1) - J_{m+1}(\mu_m^k r_1)\right)\left(Y_{m-1}(\mu_m^k r_2) - Y_{m+1}(\mu_m^k r_2)\right) -$$
$$\left(Y_{m-1}(\mu_m^k r_1) - Y_{m+1}(\mu_m^k r_1)\right)\left(J_{m-1}(\mu_m^k r_2) - J_{m+1}(\mu_m^k r_2)\right) = 0 \qquad (36)$$

Viewing this as a function of μ_m^k, the values that are able to satisfy the boundary conditions can thus be found by hunting for zeros. The ratio b/a can be found by applying the boundary condition (30) at either the inner or the outer wall. The amplitude and phase of the remaining constant (a or b) is arbitrary. A convenient practical choice is to set the value at the outer wall to unity, $B_m^k(r_{ow}) = 1$. In this way, the coefficient of the pressure represents the value that would be measured by a microphone at the outer wall in the absence of other radial harmonics.